Tight-binding analysis of energy-band structures in quantum wires

Y. Arakawa and T. Yamauchi
Research Center for Advanced Science and Technology, University of Tokyo, 4-6-1 Komaba, Meguro-ku, Tokyo 153, Japan

J. N. Schulman
Hughes Research Laboratories, Malibu, California 90265

(Received 11 June 1990; revised manuscript received 15 October 1990)

The tight-binding method is applied to the analysis of the energy bands of GaAs-$Al_{1-x}Ga_xAs$ quantum wires parallel to the [110] orientation. The results indicate that the effective mass of electrons parallel to the quantum wires in the lowest conduction band in a typical case studied can be as much as 50% larger than that of bulk GaAs and that in the second-lowest conduction band even larger. In the valence band, the reduced symmetry of the quantum wire causes enhanced heavy-hole–light-hole mixing and therefore increased nonparabolicities and reduced effective masses of the uppermost valence band. In a case studied this mass was reduced by a factor of 0.65 compared with a similarly dimensioned quantum well. The negative-effective-mass properties of the lower valence subbands are also increased relative to quantum wells. These changes in the energy-band structure would significantly affect mobilities, the transitions between subbands, and lasing characteristics of quantum-wire devices.

INTRODUCTION

In quantum-wire structures, quantization of the energy levels of electrons occurs in two transverse directions (parallel to the x and y axes), and a one-dimensional electron gas can be formed. In these structures, it was predicted that the electron mobility could be drastically enhanced at low temperature.[1] This enhancement results from the suppression of impurity scattering due to the two-dimensional confinement of electrons. Moreover, theoretical analysis also predicted that characteristics of semiconductor lasers, such as threshold current, modulation dynamics, and spectral properties, can be significantly improved with quantum-wire structures unless there is strong coupling between the electron wave functions in neighboring wires.[2–4] In most of these studies, however, the same effective mass as that of the GaAs bulk material was assumed for motion in the wire direction. Also, recently there have been a number of studies concerning transitions between confined subbands for the generation and absorption of radiation in the infrared wavelength range. The spectral properties are usually estimated using the above assumption for the effective masses of both subbands. This assumption is not suitable for more rigorous discussion of device characteristics.

On the other hand, the tight-binding method, in which the wave functions of electrons and holes in the quantum wires are described as linear combinations of orbitals on each atom, is now well known to be useful for analyzing the energy-band structure of quantum wells even when the wells are thin. Previous results for quantum wells have revealed that the *in-plane* (i.e., parallel to the quantum-well plane) band structures are quite different from those of the bulk states.[5–7] In addition, we recently applied this tight-binding calculation to the analysis of the conduction band.[8] The results show that in the cases considered the effective mass of electrons can be increased by a factor of 1.45 compared to the effective mass of the GaAs bulk material, which slightly reduces the advantage of using the quantum wires for high-electron-mobility transport devices. In order to clarify the characteristics of optical devices, the influence of the change in the effective mass in the direction of the quantum wires and the nonparabolicity of the energy-band structures should also be carefully examined.

In zinc-blende semiconductors such as GaAs, the orbitals that compose the bulk band structure near the band gap are well known. Near the Γ point the lowest conduction band mainly consists of s orbitals and the upper valence bands mainly consist of p orbitals. As the energy of the state departs from the zone-center energy, the contribution from the other orbital type gradually increases. The p orbitals have three directions, which can be chosen as p_x, p_y, and p_z. In the valence band, these orbitals combine to make the heavy, light, and spin-orbit split-off bands, which are relatively closely spaced in energy. The quantum confinement is effective in mixing these bands, causing dramatic changes in the band structure as compared with the bulk. In quantum wells, which have only one quantized direction, the valence-band structures have been quite well analyzed. Specifically, the in-plane effective mass of the heavy hole becomes smaller than that of the light hole. In addition, the light hole can take on a negative effective mass, depending on the subband energy spacing.[9] Also, the interaction of the subbands causes strong distortions away from the zone center. In this paper, we apply the tight-binding method

to the analysis of the energy-band structure of GaAs-$Al_{1-x}Ga_xAs$ quantum wires.

APPLICATION OF THE TIGHT-BINDING METHOD TO QUANUM WIRES

The tight-binding method has some advantages and some disadvantages as compared with other methods. Its main advantage is that it includes the actual atomic positions explicitly. It therefore automatically includes symmetry effects correctly. In terms of the band structure, this means that band mixings, splittings, degeneracies, and band crossings are relatively accurately produced. Also, the boundary conditions are automatically included and the current conservation requirement satisfied. For thin quantum wires, simplifying assumptions that other methods use, such as cylindrical or rectangular symmetry, infinite-barrier boundary conditions, or the setting of the barrier mass equal to the mass equal to the mass inside the wire may cause inaccuracies that are not a problem here, in that the quanum-wire position and boundary is simply defined by the alloy composition of the actual atoms at their actual positions. Also, anisotropies in the band structures are accurately produced and spin, especially important for the valence band, is also easily incorporated. A discussion of some of these considerations within the context of the $\mathbf{k}\cdot\mathbf{p}$ model can be found in Ref. 10.

Its main disadvantage is that the size of the Hamiltonian matrix that must be diagonalized is large and increases with the wire cross section. For the quantum well the problem of matrix size has been solved using the reduced Hamiltonian method,[6,7] but it is not straightforward to extend this to the quantum-wire case. Another disadvantage is that if only nearest-neighbor interactions are included, as is the case here, the conduction band near the X point is not well reproduced. Therefore, questions concerning Γ and X mixing in the conduction band are best dealt with using other methods.[11]

In our calculation model, the direction of the wire is parallel to [110], with the directions of confinement therefore being [001] and [$\bar{1}$10]. The coordinates are defined so that the x, y, and z directions are parallel to [001], [$\bar{1}$10], and [110], respectively. In Fig. 1, a cross-sectional view of the periodic quantum-wire structure is illustrated. Here, the thicknesses of the wells are equal to L_{Wx} and L_{Wy}, and the barriers are equal to L_{Bx} and L_{By}. This unit cell is periodically repeated in the two quantized directions with periods L_x and L_y. The periodic boundary conditions are represented by elements in the Hamiltonian matrix in the upper right and lower left corners by the Bloch phase factor times the overlap integral between orbitals in adjacent cells.

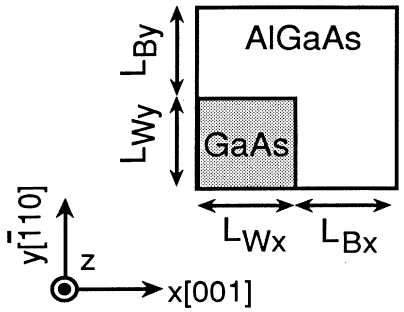

FIG. 1. Schematic cross-sectional illustration of a quantum wire.

In our calculation five orbitals per atom (s,x,y,z,s^*) are used, assuming nearest-neighbor overlaps.[12,13] This produces 20 bulk states per material, including spin. In our analysis, each atom is numbered by expanding the two-dimensional array of atoms in a cross-sectional plane of the quantum wire into a one-dimensional array. The electron wave function Ψ for the quantum wire can be expressed as a linear combination of the quantum-wire single orbital Bloch functions Ψ_J^M, where J and M label the Jth orbital on the Mth atom in the unit cell, as follows:

$$\Psi=\sum_J\sum_M C_J^M\Psi_J^M \tag{1}$$

C_J^M is the local-orbital coefficient, which is determined as an eigenvector of the following Hamiltonian matrix:

$$\langle\Psi_{J'}^{M'}|H|\Psi_J^M\rangle=\frac{1}{N}\sum_j\sum_{j'}\sum_n\sum_{n'}\sum_m\sum_{m'}\exp\{-i[(j-j')\mathbf{k}_z\cdot\mathbf{a}+(n-n')\mathbf{k}_x\cdot\mathbf{D}_x+(m-m')\mathbf{k}_y\cdot\mathbf{D}_y]\}$$
$$\times\langle\alpha_{j'}^{M'}(\mathbf{r}-\mathbf{L}_{j'n'm'}-\boldsymbol{\tau}_{M'})|H|\alpha_J^M(\mathbf{r}-\mathbf{L}_{jnm}-\boldsymbol{\tau}_M)\rangle\ , \tag{2}$$

where the vectors $\mathbf{D}$ and $\mathbf{L}_{jnm}$ are defined as follows:

$$\mathbf{D}_x=(0,0,L_x),\quad \mathbf{D}_y=\frac{L_y}{\sqrt{2}}(-1,1,0),\quad \mathbf{a}=a(1,1,0),\quad \mathbf{L}_{jnm}=j\mathbf{a}+n\mathbf{D}_x+m\mathbf{D}_y\ . \tag{3}$$

L_x and L_y are $L_{Wx}+L_{Bx}$ and $L_{Wy}+L_{By}$, respectively. a is the lattice constant. $\mathbf{k}_z$ is the wave vector in the direction of the quantum wires [110]. $\mathbf{k}_x$ and $\mathbf{k}_y$ are the wave vectors in the directions of quantization. τ_M is the position of the Mth atom in the unit cell. The α_J^M are the local atomic orbitals. The total amplitude of the quantum-wire Bloch function on the Mth atom of the crystal can be written Ψ^M and expressed by the following equation:

$$\Psi^M=\sum_J C_J^M\left[\sum_j\sum_n\sum_m\exp[-i(j\mathbf{k}_z\cdot\mathbf{a}+n\mathbf{k}_x\cdot\mathbf{D}_x+m\mathbf{k}_y\cdot\mathbf{D}_y)]\alpha_J^M(\mathbf{r}-\mathbf{L}_{jnm}-\boldsymbol{\tau}_M)\right]\ . \tag{4}$$

The summation within the parentheses in Eq. (4) is Ψ_J^M. The basis set used for the Hamiltonian matrix is

$$|s,j,\uparrow\rangle,|s,j,\downarrow\rangle,|p_x,j,\uparrow\rangle,|p_x,j,\downarrow\rangle,|p_y,j,\uparrow\rangle,|p_y,j,\downarrow\rangle,|p_z,j,\uparrow\rangle,|p_z,j,\downarrow\rangle,|s^*,j,\uparrow\rangle,|s^*,j,\downarrow\rangle ,$$

where $j=a$ or c for anion or cation. The interactions between orbitals with the same spin are

$$E_{ssj}=\langle s,j|H|s,j\rangle,\quad E_{ppj}=\langle p_x,j|H|p_x,j\rangle ,$$
$$E_{ss}=\langle s,a|H|s,c,\rangle,\quad E_{xx}=\langle p_x,c|H|p_x,a\rangle ,$$
$$E_{xy}=\langle p_x,c|H|p_y,a\rangle,\quad E_{sxac}=\langle s,a|H|p_x,c\rangle ,$$
$$E_{sxca}=\langle s,c|H|p_x,a\rangle,\quad E_{s^*s^*j}=\langle s^*,j|H|s^*,j\rangle ,$$
$$E_{s^*xac}=\langle s^*,a|H|p_x,c\rangle,\quad E_{s^*xca}=\langle s^*,c|H|p_x,a\rangle ,$$

where again $j=a$ or c. The additional interactions due to the spin-orbit component of the Hamiltonian[14] are

$$\langle p_x,j,\uparrow|H|p_y,j,\uparrow\rangle=-i\lambda_j ,$$
$$\langle p_x,j,\uparrow|H|p_z,j,\downarrow\rangle=\lambda_j ,$$
$$\langle p_y,j,\uparrow|H|p_z,j,\downarrow\rangle=-i\lambda_j ,$$
$$\langle p_z,j,\uparrow|H|p_x,j,\downarrow\rangle=-\lambda_j ,$$
$$\langle p_z,j,\uparrow|H|p_y,j,\downarrow\rangle=i\lambda_j ,$$
$$\langle p_x,j,\downarrow|H|p_y,j,\downarrow\rangle=i\lambda_j ,$$

The λ_j are chosen to reproduce the spin splitting in the valence band.[14]

Using Eqs. (1)–(4) and these matrix elements, we calculate the eigenvalues and eigenvectors of the Hamiltonian matrix to obtain the wave functions (Ψ) and the energies. The values of the parameters that were used in our calculation are summarized in Table I. They are slightly modified versions of those listed in Ref. 6. They were adjusted in order to more accurately reproduce the energy bands in the vicinity of the valence- and conduction-band edges, especially the effective masses. The effect of spin is small in the conduction band, so that in order to reduce the matrix size, it was omitted there. For the valence band the s^* components of the wave functions are very small, so that it was omitted there. The $Al_{1-x}Ga_xAs$ parameters are weighted averages of GaAs and AlAs parameters. A value for the valence-band offset of 43% of the direct-band-gap difference is used, Miller's discontinuity.[15]

TABLE I. Empirical tight-binding parameters in eV for GaAs and AlAs.

Parameter	GaAs	AlAs
$E_{ss(0,0,0)a}$	−8.4570	−7.6201
$E_{pp(0,0,0)a}$	0.9275	0.8905
$E_{ss(0,0,0)c}$	−2.7788	−1.1786
$E_{pp(0,0,0)c}$	3.5547	3.4939
$4E_{ss(1/2,1/2,1/2)}$	−6.4513	−6.6642
$4E_{xx(1/2,1/2,1/2)}$	1.9546	1.8780
$4E_{xy(1/2,1/2,1/2)}$	4.7700	3.8600
$4E_{sx(1/2,1/2,1/2)ac}$	4.6800	5.1106
$4E_{sx(1/2,1/2,1/2)ca}$	7.8500	7.1000
$E_{s^*s^*(0,0,0)a}$	8.4755	7.3905
$E_{s^*s^*(0,0,0)c}$	6.000	6.6339
$4E_{s^*x(1/2,1/2,1/2)ac}$	4.7000	4.5216
$4E_{s^*x(1/2,1/2,1/2)ca}$	7.0000	6.9000
Δ_a	0.3900	0.3500
Δ_c	0.174	0.0240

Quantum-wire conduction-band structure

First we discuss the conduction-band structure of the quantum wire. The electron effective mass in the direction of the quantum wire is a critical factor in determining election mobilities and intersubband optical transitions mentioned above. We have previously discussed the electron effective mass and its effect on electron mobility.[8] The wire had a periodic unit cell of width 90 Å ($L_x=L_y=90$ Å) and barrier layers consisting of $Al_{0.4}Ga_{0.6}As$. The results show that the electron effective mass of a quantum wire with dimensions ($L_{Wx}=35$ Å)×($L_{Wy}=30$ Å) is increased by factor of 1.45 compared to that of the GaAs bulk, and that of a quantum wire with ($L_{Wx}=50$ Å)×($L_{Wy}=50$ Å) is increased by a factor of 1.26.

For these two cases the electrons are strongly confined and the miniband width is small (less than 6 meV) in the two quantized directions. This result suggests that the increase of the effective mass in the quantum-wire direction is caused by the strong confinement for these cases. Of course when the wire width becomes small and the wave function leaks more and more into the barrier, the $Al_{1-x}Ga_xAs$ effective mass will be approached, but even for rather thin barriers the confinement in the wire is quite strong and it is the band-gap enhancement caused by the quantum confinement that increases the effective masses.

Figure 2 shows the calculated effective masses for the cases mentioned above. For decreasing L_{Wy} with, for example, L_{Wx} fixed at 50 Å, the effective mass is seen to increase. For L_{Wy} less than 10 Å the miniband width increases beyond 15 meV and the $Al_{1-x}Ga_xAs$ effective mass is approached due to wave-function smearing. For larger L_{Wy} the increase of the effective mass is caused mainly by the strong confinement.

The increase of the effective mass for the strong-confinement case can be understood from a $\mathbf{k}\cdot\mathbf{p}$ theory viewpoint. As is well known, in the simplest approximation the conduction-band effective mass is roughly proportional to the band gap in semiconductors having similar wave functions and therefore similar momentum matrix elements at $\mathbf{k}=0$. The multiplicity of subbands for

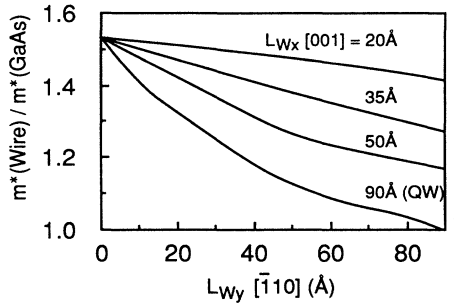

FIG. 2. The ratio of the electron effective mass of the quantum wire to that of bulk GaAs. L_{Wx} is fixed at 20, 35, 50, or 90 Å, with L_{Wy} varying.

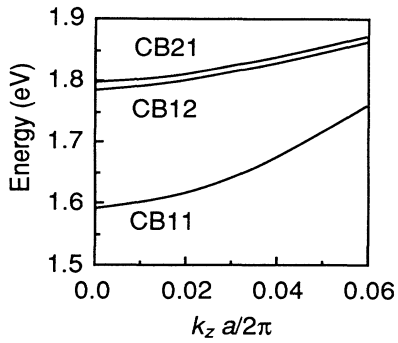

FIG. 4. Conduction-band structure in the [110] direction for a $L_{Wx}=50$ Å, $L_{Bx}=50$ Å, $L_{Wy}=40$ Å, $L_{By}=40$ Å $GaAs/Al_{0.4}Ga_{0.6}As$ quantum wire.

quantum wells and wires, especially for the valence band, complicates this picture, but for the conduction subbands, which are relatively widely spaced, the rule should still be, and is, approximately followed.

This increase in the effective mass is consistent with the change in the wave function observed for increasing confinement. $\mathbf{k}\cdot\mathbf{p}$ theory predicts that the p-orbital component of the quantum-wire wave function should increase in a simple way as the energy of the state increases above the bulk GaAs conduction-band minimum energy.[16] We calculated the wave function for a $GaAs/Al_{0.4}Ga_{0.6}As$ quantum wire with ($L_{Wx}=35$ Å)×($L_{Wy}=30$ Å) with a periodic unit of 90 Å. The electron effective mass of the wire in the lowest conduction band was 0.097 m_0. Figure 3 shows the lowest conduction-band wave function plotted through the center of the wire in the [001] direction. Here the total squared amplitudes of the s- and p-orbital components are shown. The electrons are strongly confined even in this thin-quantum-wire structure. The wave function of the p-orbital component has peaks at the $GaAs/Al_{1-x}Ga_xAs$ interface as is predicted by the boundary conditions of the simple $\mathbf{k}\cdot\mathbf{p}$ two-band model for such a state.[16]

Next we discuss the higher subbands. Here the first-, second-, and third-highest conduction bands (CB11, CB12, CB21) of the $GaAs/Al_{1-x}Ga_xAs$ quantum wire are shown in Fig. 4. The notation "CBmn" indicates the numbers of nodes plus one in the x and y directions. The zero of energy is the GaAs valence-band maximum. L_{Wx} and L_{Wy} are equal to 50 Å, and L_{Bx} and L_{By} are equal to 40 Å. The electron effective mass of CB12 is $0.108m_0$, significantly larger than that of CB11. In the analysis of optical transitions between subbands (e.g., CB11 to CB12) the electron effective masses of both bands are usually considered to be that of bulk GaAs. With such an assumption the spectral linewidth of the absorption is quite narrow because the transition energy for all k vectors has the same constant value as at $k=0$. However considering the conduction-band structures shown in Fig. 4, the transition energy does not have a constant value and in fact decreases with increasing k vector due to the larger effective mass of the higher subband. Therefore the spectral width of the absorption becomes wider in the low-energy direction below the $k=0$ band gap. In addition, increasing the n-doping concentration would cause an in-

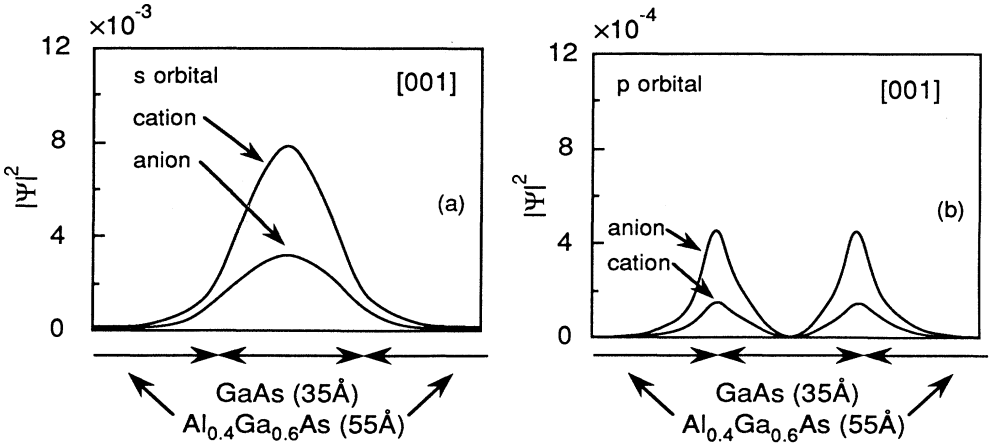

FIG. 3. The electron wave function for a $L_{Wx}=35$ Å, $L_{Bx}=55$ Å, $L_{Wy}=30$ Å, $L_{By}=60$ Å $GaAs/Al_{0.4}Ga_{0.6}As$ quantum wire plotted along a line through the wire center parallel to [001].

crease of the spectral linewidth. Further details will be discussed elsewhere.[17]

Valence-band structures of quantum wires

In the calculation of the valence-band structure pure AlAs barriers are used.

Bulk GaAs and AlAs band structures

First we show the bulk GaAs and AlAs valence-band structures for comparison with that of the quantum wires. Figure 5 shows the valence-band structures of GaAs and AlAs in the [110] direction. The units of k_z are $2\pi/a$, where a is the conventional zinc-blende unit-cell length. The zero of energy is the GaAs valence-band maximum. The AlAs valence-band maximum is at 0.676 eV corresponding to the 43% offset rule.

The valence-band structures of GaAs/AlAs quantum wires

We calculated the valence-band structures of three quantum wires with varying amounts of quantum confinement as determined by the layer thicknesses. The three wires had varying ratios of wire and barrier thickness, with the total periodic cell widths held constant at $L_x = L_y = 62$ Å. From this we will see that the confinement in the two directions significantly affects the valence-band structures. The nonparabolicities in the valence bands are even greater than that in quantum wells due to the greater mixing of bulk heavy- and light-hole-like characteristics. In fact, there is heavy-hole–light-hole mixing even at $k = 0$ so that the bands cannot be distinguished in this way. This can be understood by regarding the quantum-wire wave function as a linear combination of bulk states with both k_x and k_y not equal to zero. Since such a general bulk k point has no special symmetry, bulk heavy- and light-hole states are mixed freely in the wire. This is especially true for wires with close to equal dimensions in the x and y directions.[10] The subband spacings are also important in determining the mixings and nonparabolicities, just as they are in quantum wells.

Figure 6 shows the valence-band structures for the three representative cases. Table II lists the energies of

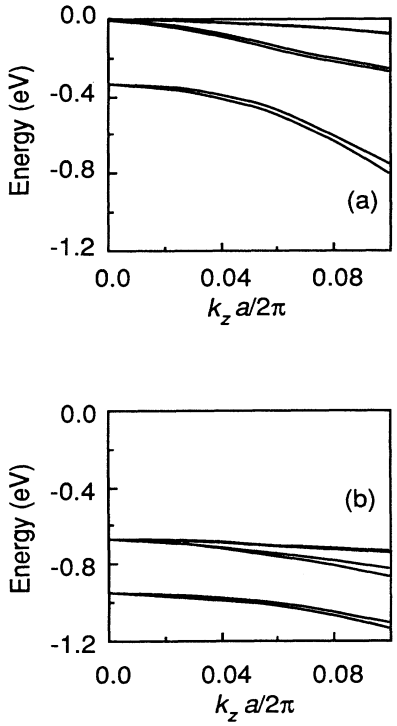

FIG. 5. Valence-band structure in the [110] direction for (a) bulk GaAs and (b) AlAs. The zero of energy is the GaAs valence-band maximum.

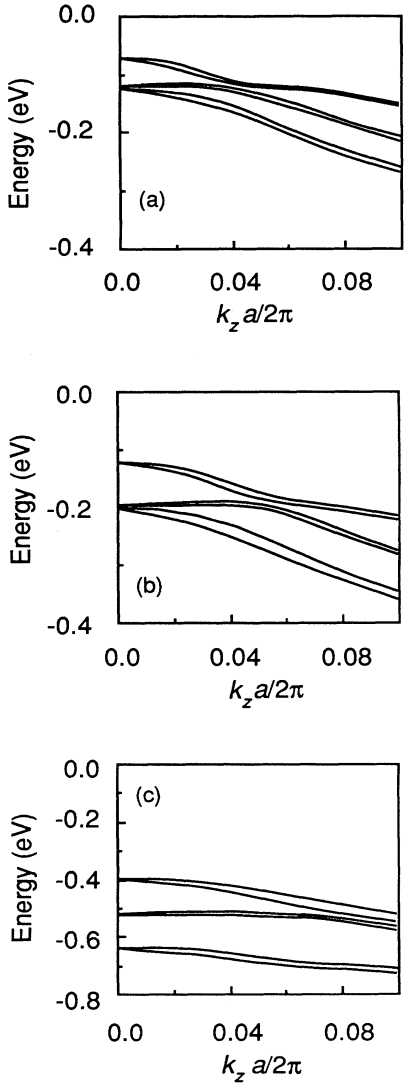

FIG. 6. Valence-band structure in the [110] direction for GaAs/AlAs quantum wires. (a) $L_{Wx} = L_{Wy} = 45$ Å, $L_{Bx} = L_{By} = 17$ Å, (b) $L_{Wx} = L_{Wy} = 31$ Å, $L_{Bx} = L_{By} = 31$ Å, (c) $L_{Wx} = L_{Wy} = 11$ Å, $L_{Bx} = L_{By} = 51$ Å.

TABLE II. The energy of the top three valence bands of a GaAs/AlAs quantum wire whose periodic unit is 62 Å. Energies are in eV.

L_{Wx}, L_{Wy}	L_{Bx}, L_{By}	VB1	VB2	VB3
45 Å	17 Å	−0.0722	−0.1201	−0.1264
31 Å	31 Å	−0.1213	−0.1987	−0.2036
11 Å	51 Å	−0.3981	−0.5192	−0.6434

the top three valence bands at the zone center for each. The dimensions of the three cases are (a) $L_{Wx}=L_{Wy}=45$ Å, $L_{Bx}=L_{By}=17$ Å; (b) $L_{Wx}=L_{Wy}=31$ Å, $L_{Bx}=L_{By}=31$ Å; and (c) $L_{Wx}=L_{Wy}=11$ Å, $L_{Bx}=L_{By}=51$ Å. The confinement is larger for the larger wires, resulting in energies closer to the bulk GaAs valence-band maximum and more closely spaced subbands. The simultaneous decrease in barrier width with increasing wire width is a secondary unimportant effect here. For cases (a) and (b) the energy of VB2 (the second uppermost valence band) is located close to VB3 (the third uppermost valence band) near the zone center causing a strong $\mathbf{k}\cdot\mathbf{p}$ repulsion between the two and a resulting negative effective mass for VB2 (relative to the normal sign of the mass) similar to that found in quantum wells.[9] In addition, the repulsion between VB2 and VB3 causes VB2 and VB1 (the uppermost valence band) to anticross away from the zone center. On the other hand, as the width of the GaAs wire region becomes smaller as in case (c), the quantized energy of VB3 at the zone center approaches the AlAs valence-band barrier height, the wave function of VB3 spreads into the barrier layers, and the separation of the quantized energy levels is relatively large. In this case the mixing between bands becomes weak. Thus the degree of confinement affects the valence-band structures through the mixing of the bands with each other.

Comparison between quantum wires and quantum wells

Next we compare the valence-band structures of quantum wires and quantum wells. The calculated valence-band structure of a 40×40 Å^2 quantum wire in the direction of the wire is shown in Fig. 7. The result for the [110] direction in-plane dispersion of the valence band of

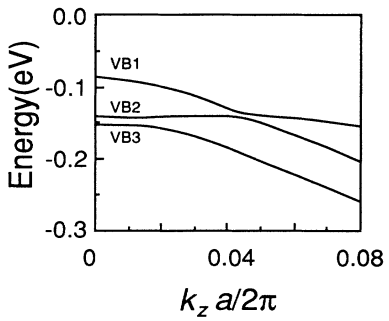

FIG. 7. Valence-band structure in the [110] direction for a $L_{Wx}=40$ Å, $L_{Bx}=34$ Å, $L_{Wy}=40$ Å, $L_{By}=34$ Å GaAs/AlAs quantum wire.

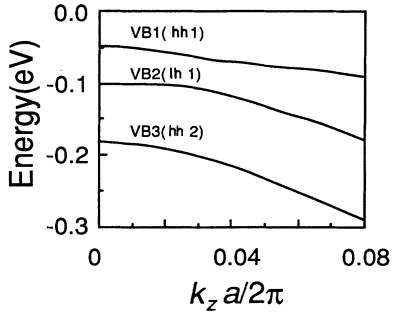

FIG. 8. Valence-band structure in the [110] direction for a GaAs(40 Å)/AlAs(34 Å) quantum well whose orientation is (001).

a GaAs (40 Å)-AlAs(34 Å) quantum well whose plane is normal to (001) [i.e., the direction of quantization is parallel to (001)] is shown in Fig. 8. For simplicity we have here plotted the average of the energies of the two closely spaced spin-split band pairs. As can be seen, in the quantum-well structure strong nonparabolicities of the dispersion curve are observable. Moreover, the effective masses of the heavy holes 1 and 2 (VB1 and VB3) in the in-plane directions are much smaller than that of the light hole (VB2), in contrast to the quantized direction. In addition, the effective mass of light-hole 1 (VB2) in the in-plane direction is slightly negative. These properties are well-known typical features of quantum wells.[5–7]

On the other hand, the calculation for the quantum wire shown in Fig. 7 indicates that both nonparabolicites and the negative-effective-mass nature of the second uppermost valence band (VB2) are more enhanced compared to that of the similarly dimensioned quantum well. The effective mass of the first uppermost valence band (VB1) is 65% of that of the quantum well. In Table III, the values of the effective masses in the lowest conduction band and the uppermost valence band are summarized. In addition, the results indicate that the effective mass of the third band, VB3, is also slightly negative. VB2 approaches VB3 at the zone center and approaches VB1 a little away from zone center. Thus the valence bands of the quantum wires are strongly mixed with one another.

In Table IV, the miniband width in the confined directions of each subband in the valence band is summarized for the quantum well and wire. In the quantum well, the miniband width of the light hole (VB2) is larger than that

TABLE III. Summary of the effective masses in the lowest conduction band (CB1) and the uppermost valence band (VB1) of the 40×40 Å^2 GaAs/AlAs quantum wire, (001) GaAs(40 Å)/AlAs(34 Å) quantum well, and bulk GaAs. The direction is [110]. Here, m_0 is the mass of an electron.

	CB1	VB1
Wire	$0.103m_0$	$0.168m_0$
Well	$0.082m_0$	$0.258m_0$
GaAs	$0.066m_0$	$0.749m_0$

TABLE IV. Miniband width of valence bands in meV for the quantum wires shown in Fig. 7 and (001) GaAs(40 Å)/AlAs(34 Å) quantum wells.

Direction	CB1	VB1	VB2	VB3
Wire [001]	0.47	0.0726	0.020	0.252
Wire [$\bar{1}$10]	0.98	0.0847	0.059	0.775
Well [001]	0.57	0.0070	0.781	0.050

of the heavy holes (VB1 and VB3), which is a typical feature of quantum wells. On the other hand, in the quantum wire the miniband width of VB2 is almost the same as that of VB1 and is much smaller than that of VB3. Characterization of the wire subbands as heavy- or light-hole-like must be done with caution, however, due to the heavy-hole–light-hole mixing. The complications of the valence-band structures would be expected to influence the lasing properties of wires, especially in so far as the density of states is affected. Details will be discussed eleswhere.[17]

CONCLUSION

In conclusion, we have calculated the energy bands of GaAs-$Al_{1-x}Ga_xAs$ quantum wires that are parallel to the [110] direction using the tight-binding method. In the conduction bands of GaAs-$Al_{0.4}Ga_{0.6}As$ quantum wires, the results indicate that the confinement of electrons increases the effective mass in the wire direction due to the increased band gap. The effective mass of the quantum wire with a 50×50 Å^2 cross section is 1.27 times as large as that of bulk GaAs, while the miniband width is quite small. Moreover, the electron effective masses of higher subbands are not the same as the lowest subband, but are indeed significantly larger. These results would influence the electron mobility of quantum wires and the absorption coefficients of transitions between the subbands. In the valence band, the results indicate that strong nonparabolicities and band mixings are occurring, depending on subband spacings, due to the decreased symmetry of the wire relative to the well. The effective mass of VB1 in a case studied was reduced by 65% relative to that of a similarly dimensioned quantum well, resulting in a value of $0.168m_0$. Also, the negative effective mass of VB2 was enhanced and that of VB3 became slightly negative. The results obtained in this paper suggest the importance of considering the band structure in the design of quantum-wire devices utilizing valence bands such as semiconductor lasers.[17]

ACKNOWLEDGMENTS

We would like to express our thanks for the support of our research work by Ogasawara Foundation, Matsuda Foundation, University-Industry Joint Project on "Mesocopic Electronics," and a Grant-in-Aid from the Ministry of Education, Science and Culture.

[1]H. Sakaki, Jpn. J. Appl. Phys. **19**, L735 (1980).
[2]Y. Arakawa, K. Vahala, and A. Yariv, Appl. Phys. Lett. **45**, 950 (1984).
[3]M. Asada, Y. Miyamoto, and Y. Suematsu, IEEE J. Quantum Electron. **QE-22**, 1915 (1986).
[4]Y. Arakawa and A. Yariv, IEEE J. Quantum Electron. **QE-22**, 1887 (1986).
[5]Y. C. Chang and J. N. Schulman, Appl. Phys. Lett. **43**, 536 (1983).
[6]J. N. Schulman and Y. C. Chang, Phys. Rev. B **31**, 2056 (1985).
[7]Y. C. Chang and and J. N. Schulman, Phys. Rev. B **31**, 2069 (1985).
[8]T. Yamauchi, Y. Arakawa, and J. N. Schulman, Appl. Phys. Lett. **57**, 1224 (1990).
[9]G. D. Sanders and Y. -C. Chang, Phys. Rev. B **31**, 6892 (1985).
[10]D. S. Citrin and Y. -C. Chang, Phys. Rev. B **40**, 5507 (1989).
[11]K. B. Wong, M. Jaros, and J. P. Hagon, Phys. Rev. B **35**, 2463 (1987).
[12]P. Vogl, H. P. Hjalmarson, and J. D. Dow, J. Phys. Chem. Solids **44**, 365 (1983).
[13]C. S. Lent, M. A. Bowen, J. D. Dow, R. S. Allgaier, O. F. Sankey, and E. S. Ho, Supperlatt. Microstruct. **2**, 491 (1986).
[14]D. J. Chadi, Phys. Rev. B **16**, 790 (1977).
[15]R. C. Miller, D. A. Kleinman, and A. C. Gossard, Phys. Rev. B **29**, 7085 (1984).
[16]G. Bastard, Phys. Rev. B **25**, 7584 (1982).
[17]T. Yamauchi, Y. Arakawa, and T. Takahashi (unpublished).